SECURITY CLASSIFICATION OF THIS PAGE

REPORT DOCUMENTATION PAGE

19960417 139

1a. REPORT SECURITY CLASSIFICATION Unclassified	1b. RESTRICTIVE MARKINGS
2a. SECURITY CLASSIFICATION AUTHORITY	3. DISTRIBUTION/AVAILABILITY OF REPORT Unclassified/Unlimited
2B. DECLASSIFICATION/DOWNGRADING SCHEDULE	
4. PERFORMING ORGANIZATION REPORT NUMBER(S) Technical Report #9	5. MONITORING ORGANIZATION REPORT NUMBER(S)
6a. NAME OF PERFORMING ORGANIZATION University of Minnesota 6b. OFFICE SYMBOL (if applicable)	7a. NAME OF MONITORING ORGANIZATION Office of Naval Research
6C. ADDRESS (City, State, and Zip Code) Dept. of Chemical Engineering &Materials Science University of Minnesota Minneapolis, MN 55455	7B. ADDRESS (City, State and Zip Code) 800 Quincy Street North Arlington, VA 22217-5000
8a. NAME OF FUNDING/SPONSORING ORGANIZATION Office of Naval Research 8b. OFFICE SYMBOL (if applicable) ONR	9. PROCUREMENT INSTRUMENT IDENTIFICATION NUMBER Contract No. N/N00014-93-1-0563
8c. ADDRESS (City, State, and Zip Code) 800 Quincy Street North Arlington, VA 22217-5000	10. SOURCE OF FUNDING NUMBERS PROGRAM ELEMENT NO. / PROJECT NO. / TASK NO. / WORK UNIT ACCESSION NO

11. TITLE (Include Security Classification)

Electrochemical Annealing and Friction Anisotropy of Domains in Epitaxial Molecular Films

12. PERSONAL AUTHOR(S)

Julie A. Last and Michael D. Ward

13a. TYPE OF REPORT	13b. TIME COVERED	14. DATE OF REPORT (Year, Month, Day)	15. PAGE COUNT
Technical	FROM 5/1/95 TO 6/30/96	96/4/8	17

16. SUPPLEMENTARY
to be published in Advanced Materials

17. COSATI CODES			18. SUBJECT TERMS (Continue on reverse if necessary and identify by block number)
FIELD	GROUP	SUB-GROUP	Organic Condustor, Atomic Force Microscopy, Scanning Electron Microscopy, Nucleation

19. ABSTRACT (CONTINUE ON REVERSE AND IDENTIFY BY BLOCK NUMBER

Electrochemical annealing of domain boundary defects in an epitaxial monolayer whose structure mimics the (001) layers of the organic superconductor β-bis(ethylenedithio)tetrathiafulvalene trioxide, $(ET)_2I_3$, has been visualized in situ using real-time atomic force microscopy. These defects are observed readily by lateral force imaging and high resolution contact mode imaging reveals that the domains are oriented at angles of $\pm n60$ because of epitaxy with the HOPG substrate. The frictional contrast between domains is due to the anisotropy molecular field encountered by the tip and is a direct consequence of the crystalline order of the rigid monolayer. Potential cycling about the deposition potential resulted in a reduction in the number of domains, with the smaller domains eventually adopting the orientation of surrounding larger ones, ultimately forming large (>15 μm^2) defect free monolayers. This demonstrates that the defect density of redox-active molecular films can be reduced by relatively simple means.

20. DISTRIBUTION/AVAILABILITY OF ABSTRACT	21. ABSTRACT SECURITY CLASSIFICATION
☐ UNCLASSIFIED/UNLIMITED ☐ SAME AS RPT ☐ OTIC USERS	Unclassified
22a. NAME OF RESPONSIBLE INDIVIDUAL Michael D. Ward	22b. TELEPHONE (Include Area Code) (612) 625-3062 / 22C. OFFICE SYMBOL

DD FORM 1473, 84 MAR 83 APR edition may be used until exhausted. All other editions are obsolete.

SECURITY CLASSIFICATION OF THIS PAGE
Unclassified

OFFICE OF NAVAL RESEARCH

Contract N00014-93-1-0563

Technical Report No. 9

"Electrochemical Annealing and Friction Anisotropy of Domains in Epitaxial Molecular Films"

by

Julie A. Last and Michael D. Ward

to be published in

Advanced Materials

Department of Chemical Engineering and Materials Science
University of Minneapolis
421 Washington Avenue SE
Minneapolis, MN 55455

April 1996

Electrochemical Annealing and Friction Anisotropy of Domains in Epitaxial Molecular Films**

Julie A. Last and Michael D. Ward*

Abstract

Electrochemical annealing of domain boundary defects in an epitaxial monolayer whose structure mimics the (001) layers of the organic superconductor β-bis(ethylenedithio)tetrathiafulvalene triiodide, $(ET)_2I_3$, has been visualized *in situ* using real-time atomic force microscopy. These defects are observed readily by lateral force imaging and high resolution contact mode imaging reveals that the domains are oriented at angles of $\pm n60^\circ$ because of epitaxy with the HOPG substrate. The frictional contrast between domains is due to the anisotropic molecular field encountered by the tip and is a direct consequence of the crystalline order of the rigid monolayer. Potential cycling about the deposition potential resulted in a reduction in the number of domains, with the smaller domains eventually adopting the orientation of surrounding larger ones, ultimately forming large (> 15 μm^2) defect free monolayers. This demonstrates that the defect density of redox-active molecular films can be reduced by relatively simple means.

---

[*] Prof. M.D. Ward, J.A. Last
Department of Chemical Engineering and Materials Science
151 Amundson Hall
421 Washington Ave S.E.
University of Minnesota
Minneapolis, Minnesota 55455

[**] The authors acknowledge the financial support of the Office of Naval Research. Helpful discussions with Dr. Andrew C. Hillier and Christopher M. Yip are also acknowledged.

Submitted to *Advanced Materials*, March 26,1996

The formation of high quality thin films is essential for many electronic and optical technologies.[1] While substantial advances have been made with conventional elemental and inorganic materials there is increasing interest in molecular films, largely based on the premise that electrical and optical properties can be manipulated by molecular design and control of supramolecular organization on substrate surfaces. For example, vapor deposition and molecular beam techniques have been employed to fabricate epitaxial films of 3,4,9,10-perylenetetracarboxylic dianhydride (PTCDA) on graphite,[2,3,4,5] and films of organic dyes such as copper phthalocyanine on graphite, SnS_2 and MoS_2.[6,7,8] Langmuir-Blodgett films[9,10,11] and self-assembled monolayers with redox active components[12,13,14] have been investigated owing to the possibility of two-dimensional electronic properties. However, applications based on these films is likely to be limited by their high defect densities and poor lateral ordering.[15,16]

Molecular crystals commonly possess two-dimensional layered structures with strong bonding within the layers and relatively weak van der Waals bonding between layers.[17] Numerous examples of molecular crystals exhibit electrical and superconductivity,[18] ferromagnetism,[19] and nonlinear optical behavior.[20] This suggests that these materials can provide a new paradigm for the design of robust, highly ordered crystalline films with predictable molecular-scale architecture and novel electronic properties.[21,22] Indeed, recent studies in our laboratory have demonstrated that molecular films based on conducting and superconducting organic charge-transfer salts have structures which mimic that of specific crystal planes of their bulk counterparts.[23,24,25,26] For example, *in situ* atomic force microscopy (AFM) revealed that electrochemical oxidation of bis(ethylenedithiolo)tetrathiafulvalene (ET) in the presence of I_3^- led to formation of a robust molecularly thick film on highly oriented pyrolytic graphite (HOPG).[25,26] The thickness and lattice parameters of the film indicated the formation of a monolayer with a structure mimicking the (001) layer of β-$(ET)_2I_3$, a superconducting phase. Indeed, further growth on top of this monolayer led to selective formation of bulk

crystals of this polymorph. The azimuthal orientation of the monolayer and subsequently formed bulk crystals was consistent with coincidence of the (001) β-$(ET)_2I_3$ layer with the HOPG substrate, a condition which was confirmed by an analytical two-dimensional lattice match calculation.[27,28] However, monolayer growth was accompanied by the formation of domains with different orientations due to the symmetry of the HOPG substrate, leading to domain boundary defects which may serve as barriers to electron transport in the two-dimensional layers. We describe herein observation of frictional anisotropy during lateral force imaging of these domains and an "electrochemical annealing" process that reduces the number of domains in (001) β-$(ET)_2I_3$ monolayers. This procedure results in essentially defect-free films, and should be applicable generally to redox-active molecular films.

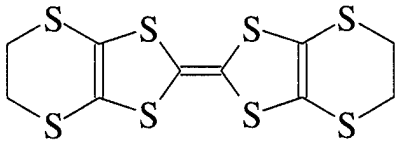

ET

Electrochemical oxidation of ET at 650 mV (vs. Ag/AgCl) in acetonitrile containing 0.1 M n-$Bu_4{}^+N$ $I_3{}^-$ results in growth of a monolayer with a structure mimicking the (001) layer of β-$(ET)_2I_3$ on an HOPG electrode, which can be observed directly by AFM.[25,26] Real-time investigations revealed that a complete monolayer was formed by coalescence of separate growing monolayer domains. Lateral force imaging, which relies on lateral twisting of the AFM cantilever due to friction with the sample, revealed an enhanced contrast at the domain boundaries when imaging was performed at 90° (Figure 1a). The AFM data also revealed identical heights (15.5 Å) and in-plane lattice parameters ($\mathbf{b_1}$ = 6.6 Å, $\mathbf{b_2}$ = 9.1 Å, β = 110°) which we previously assigned to a monolayer with structural features identical to the (001) layer of β-$(ET)_2I_3$. High resolution data revealed a 60° orientational difference between the monolayer lattices of adjacent domains. This is

consistent with the symmetry of the HOPG substrate and the azimuthal orientation in which coincidence of the monolayer, confirmed by AFM data and modeling of the interface,[25,26] is achieved at $\mathbf{b_1} = 4.0\mathbf{a_1} + 2.0\mathbf{a_2}$ and $\mathbf{b_2} = -4.0\mathbf{a_1} + 3.3\mathbf{a_2}$, where $\mathbf{a_1}$ and $\mathbf{a_2}$ are the in-plane lattice vectors of HOPG (Figure 2). The enhancement of friction at the domain boundaries can be attributed to disorder in these regions owing to orientational mismatch, which may lead to a decrease in the rigidity of the film at the boundaries. Previous studies have suggested that friction is greater for domains with lesser order and lower moduli due to greater penetration of the tip in softer phases.[29, 30]

[Figure 1]

[Figure 2]

The lateral force images acquired at an angle of 90° exhibited perceptible, but small, differences in friction between domains. In contrast, lateral force imaging at an angle of 0° revealed substantial differences in friction between the domains (Figure 1b). The observation of friction contrast must be due to orientation differences between domains, as the domains are of identical composition and structure. That is, the differences must be due to frictional anisotropy as the tip moves along the surface of the β-ET_2I_3 monolayer, which is structurally anisotropic with respect to the direction of tip motion (Figure 2). This also indicates that the monolayer must be rigid on the time scale of the tip motion and must be highly ordered, consistent with the observation of molecular contrast for this monolayer. We presume that friction experienced by the tip is due to atomistic stick-slip, as lattice-over-lattice sliding in which a flake of the sample picked up by the tip is moved across the sample is unlikely here.[31] The anisotropy of the molecular field of the (001) layer will result in differing degrees of stick-slip on differently oriented domains for a given tip moving in a fixed direction. Frictional anisotropy has been observed previously in only a limited number of examples, including domains of a poly(oxymethylene) single crystal[32]

and a lipid bilayer.[33] Images taken at both 0° and 90° reveal domains of identical shapes, although more domains are evident in the 90° scan. High resolution imaging reveals that a small number of domain boundaries are associated with translational displacement between identically oriented domains. Under this condition, domain boundaries would be evident even though the contrast of the domains would be identical. Such a condition may account for the observation of additional domains at the 90° scanning angle.

Application of a potential which was cathodic of the monolayer stripping potential (550 mV vs Ag/AgCl) resulted in film dissolution at the domain boundaries (Figure 3) due to the higher free energy of the β-$(ET)_2I_3$ monolayer at the domain boundaries.[34] Dissolution generally was more rapid at the boundaries of domains having larger perimeter-to-area ratios. Cycling the film potential between 550 mV and 675 mV vs Ag/AgCl, which is cathodic of the stripping potential and anodic of the deposition potential, respectively, resulted in progressive growth of the larger domains at the expense of smaller domains (Figure 4). For example, the areas of domains 1, 2, and 3 in Figure 4 decrease upon potential cycling, while numerous domains in the center of the scanned region disappear completely. Domains 4, 5, and 6 increase in area, with domains 5 and 6 annealing into a single domain filling most of the scan area, resembling Ostwald ripening.[1] The result is an overall reduction of the total length of domain boundaries, with the data in Figures 4a, 4b, and 4c exhibiting total domain boundary lengths of 23.9, 18.7 and 14.3 μm, respectively. Additional experiments have demonstrated that incompletely dissolved domains regrow with the same orientation as the smaller domain, but growth from surrounding larger domains intrudes on the region previously occupied by the domain. This results in a progressive movement of the domain boundary toward the center of the smaller domain until the annealing is complete (Figure 5). Secondary nucleation events in the dissolved regions were never observed.

[Figure 3]

[Figure 4]

[Figure 5]

These observations illustrate that monolayer films with potentially novel electronic properties can be prepared by electrochemical routes, and that these films can be annealed by simple potential cycling about the deposition and dissolution potentials. The ability to visualize these processes *in situ* and in real time with AFM enables elucidation of the role of epitaxy in domain formation and the influence of domain size on the dynamics of annealing. The combination of electrochemical growth and annealing can enable the fabrication of relatively defect-free molecular films on substrates with non-planar geometries.

Experimental

Atomic force microscopy experiments were performed using a Digital Instruments, Inc. Nanoscope III scanning probe microscope and Si_3N_4 tips (quoted spring constant of 0.06 Nm^{-1}). A piezoelectric scanner with a maximum lateral scanning range of 15 μm x 15 μm was used for imaging. All images shown were obtained in lateral force mode, at tip scan rates ranging from 2 to 10 Hz. Data were collected using Digital Instruments Nanoscope III version 4.1 software and were low-pass filtered once. Image analysis was performed with the Nanoscope III and with NIH Image version 1.59b2 (available by anonymous FTP at zippy.nimh.nih.gov) software. Electrodeposition of the monolayers was performed in acetonitrile solutions containing 0.5 mM ET (Aldrich) and 2 mM tetrabutylammonium triiodide (n-$Bu_4N^+I_3^-$). The n-$Bu_4N^+I_3^-$ was prepared by addition of 5 g (0.01354 mol) n-$Bu_4N^+I^-$ (Aldrich) to 120 ml of 1.7 M KI (Aldrich), followed by addition of 3.44 g I_2. The resulting dark brown solution and deep purple oil layer was stirred at 70°C for approximately 10 minutes and allowed to cool to room temperature, resulting in the formation of dark black solids which were filtered, collected and rinsed

with distilled water. Recrystallization from hot methanol and drying *in vacuo* afforded dark black plate-like crystals of $TBAI_3$.

Electrodepositions were performed in an AFM fluid cell (Digital Instruments) equipped with ports for fluid entry and exit. Freshly cleaved highly oriented pyrolytic graphite (HOPG) was used as the substrate and working electrode, and platinum counter and quasi-reference electrodes were inserted through the outlet port of the fluid cell. Potential cycling was performed by applying a square wave with a homemade function generator. Potential limits were chosen based on the potential at which monolayer deposition and dissolution was observed in the scanning region. Typically, deposition first occurred at approximately 650 mV vs. Ag/AgCl, with the monolayer remaining stable at 620 mV. The potential was cycled approximately 620±75 mV, with the anodic potential held for approximately 20 seconds and the cathodic potential held for approximately 15 seconds.

Figure Captions

Figure 1. (A) Lateral force images of a completely formed monolayer with a structure mimicking the (001) layer of β-$(ET)_2I_3$ acquired with the cantilever oriented at 90° with respect to the scan direction (horizontal). In this mode the domain boundaries are pronounced. (B) Lateral force images of a completely formed β-$(ET)_2I_3$ monolayer acquired with the tip oriented at 0° with respect to the scan direction (vertical). In this mode the frictional contrast between differently oriented domains is accentuated.

Figure 2. (A) Schematic representation of two adjacent β-ET_2I_3 domains, separated by a domain boundary, on the HOPG substrate (only the ethylene ends of the ET molecules in contact with the substrate are shown for clarity). The domain boundary is indicated by a dashed line. The domains have a 60° orientational difference, as deduced from real space AFM data and Fourier transforms, the latter being illustrated below. Each domain is coincident with the HOPG substrate, with $\mathbf{b_1} = 4.0\mathbf{a_1} + 2.0\mathbf{a_2}$ and $\mathbf{b_2} = -4.0\mathbf{a_1} + 3.3\mathbf{a_2}$, where $\mathbf{a_1}$ and $\mathbf{a_2}$ are the in-plane lattice vectors of HOPG. This orientation results in an angle of 19° between the monolayer lattice vector $\mathbf{b_1}$ and the HOPG lattice vector $\mathbf{a_1}$. The coincidence implies a non-primitive $1\mathbf{b_1} \times 3\mathbf{b_2}$ supercell (shown here) which is commensurate with the HOPG substrate. (B) A space filling model of two adjacent domains of a (001) β-ET_2I_3 layer as viewed normal to the layer. Frictional contrast between differently oriented domains is observed because of their differently oriented molecular fields.

Figure 3. Lateral force AFM images illustrating dissolution of a (001) β-$(ET)_2I_3$ monolayer. (A) t = 0, (B) t = 30 sec. Dissolution occurs preferentially at the boundaries of the smaller domains. The domain boundaries are highlighted here with dashed lines for clarity.

Figure 4. Sequence of AFM images illustrating the electrochemical annealing of a (001) β-$(ET)_2I_3$ monolayer acquired in lateral force mode *in situ* during potential cycling between 550 and 650 mV (vs. Ag/AgCl) at (A) t = 0, (B) t = 22 min., (C) t = 41 min. The data was collected with the tip oriented at 90° with respect to the direction of tip motion. The number and the overall perimeter of the domain boundaries decrease with time. The domain boundaries are highlighted here with dashed lines for clarity. The numbered domains are discussed in the text.

Figure 5. Schematic representation of electrochemical annealing. Differently oriented domains are represented by differently oriented line patterns, and the dashed line refers to the boundary of the original domain. (1) Upon application of a cathodic potential, -E, monolayer dissolution begins at the domain boundary. (2), (3) If the cathodic potential is applied for an amount of time sufficient for complete domain dissolution, subsequent application of an anodic potential leads to growth of the surrounding monolayer with no new nucleation occurring where the original domain existed, thus affording a nominally defect-free film. (4) If a small island remains after domain dissolution, upon potential reversal monolayer growth occurs at the edges of the island and the surrounding terrace. In this case, the newly formed domain boundary has a smaller perimeter than before dissolution. (5) Continued potential cycling results in eventual disappearance of the smaller domain.

References

[1] R.W. Vook, *International Metals Review*, **1982**, *27*, 209.

[2] S.R. Forrest, Y. Zhang, *Phys. Rev. B*, **1994**, *49*, 11297.

[3] S.R. Forrest, P.E. Burrows, E.I. Haskal, F.F. So, *Phys. Rev. B*, **1994**, *49*, 11309.

[4] C. Ludwig, B. Gompf, W. Glatz, J. Petersen, W. Eisenmenger, M. Mobus, U. Zimmermann, N. Karl, *Z. Phys. B*, **1992**, *86*, 397.

[5] C. Ludwig, B. Gompf, J. Petersen, R. Strohmaier, W. Eisenmenger, *Z. Phys. B*, **1994**,*93*, 365.

[6] A. Hoshino, S. Isoda, H. Kurata, T. Kobayashi, *J. Appl. Phys.* **1994**, *76*, 4113.

[7] C. Ludwig, R. Strohmaier, J. Petersen, B. Gompf, W. Eisenmenger, *J. Vac. Sci. Technol. B*, **1994**, *12*, 1963.

[8] K.W. Nebesny, G.E. Collins, P.A. Lee, L.-K. Chau, J. Danziger, E.Osburn, N.R. Armstrong, *Chemistry of Materials*, **1991**, *3*, 829.

[9] A. Ulman, *An Introduction to Ultrathin Organic Films From Langmuir-Blodgett to Self Assembly*, Academic Press, Inc., New York **1991**.

[10] B.Tieke, *Advanced Materials*, **1990**, *2*, 222.

[11] M.R. Bryce, M.C. Petty, *Nature*, **1995**, *374*, 771.

[12] C.M. Yip, M.D. Ward, *Langmuir*, **1994**, *10*, 549.

[13] M. Matsumoto, T. Nakamura, E. Manda, Y. Kawabata, *Thin Solid Films*, **1988**, *160*, 61.

[14] A.S. Dhindsa, Y.-P. Song, J.P. Badyal, M.R. Bryce, Y.M. Lvov, M.C. Petty, J. Yarwood, *J. Chem. Mater.*, **1992**, *4*, 724.

[15] J. Garnes, D.K. Schwartz, R. Viswanathan, J.A.N. Zasadzinski, *Synth. Met.* **1993,** *55-57*, 3795.

[16] L.F. Chi, H. Fuchs, R.R. Johnston, H. Ringsdorf, *Thin Solid Films* **1994,** *242*, 151.

[17] A. Uhlman, R.P. Scaringe, *Langmuir*, **1992**,*8*, 894.

[18] J. Miller, *Extended Linear Chain Compounds*, vol. 1-3, Plenum Press, New York **1982-84**.

[19] J.S. Miller, A.J. Epstein, W.M. Reiff, *Science*, **1988**, *240*, 40.

[20] J. Zyss, G. Tscoucaris, *Structure and Properties of Molecular Crystals* (Ed: M. Pierrot), Elsevier, Amsterdam **1990**.

[21] *Molecular Electronic Devices* (Ed: F.L. Carter), Marcel Decker, New York **1982**.

[22] *Molecular Electronics* (Ed: G.J. Ashwell), John Wiley & Sons, New York **1992**.

[23] J. Hossick-Schott, M.D. Ward, *J. Am. Chem. Soc.*, **1994**, *116*, 6806.

[24] J. Hossick-Schott, C.M. Yip, M.D. Ward, *Langmuir*, **1995**, *11*, 177.

[25] A.C. Hillier, J.B. Maxson, M.D. Ward, *Chem. Mater.*, **1994**, *6*, 2222.

[26] A.C. Hillier, J. Hossick-Schott, *Adv. Mater.*, **1995**, *7*, 409.

[27] A.C. Hillier, M.D. Ward, manuscript in preparation.

[28] A.C. Hillier, Ph.D. Thesis, University of Minnesota, **1995**.

[29] R. M. Overney, E. Meyer, J. Frommer, H. J. Guntherodt, M. Fujihara, H. Takano, Y. Gotoh, *Langmuir*, **1994**, *10*, 1281.

[30] X. Xiao, J. Hu, D.H. Charych, M. Salmeron, *Langmuir*, **1996**, *12*, 235.

[31] C. M.Mate, G. M. McClelland, R. Erlandsson, S. Chiang, *Phys. Rev. Lett*, **1987**, *59*, 1942.

[32] R. Nisman, P. Smith, G. J. Vancso, *Langmuir*, **1994**, *10*, 1667.

[33] R.M. Overney, H. Takano, M. Fujihira, *Phys. Rev. Lett.*, **1994**, *72*, 3546.

[34] M. Ohring, *The Materials Science of Thin Films*, Academic Press, Inc., New York **1992**.

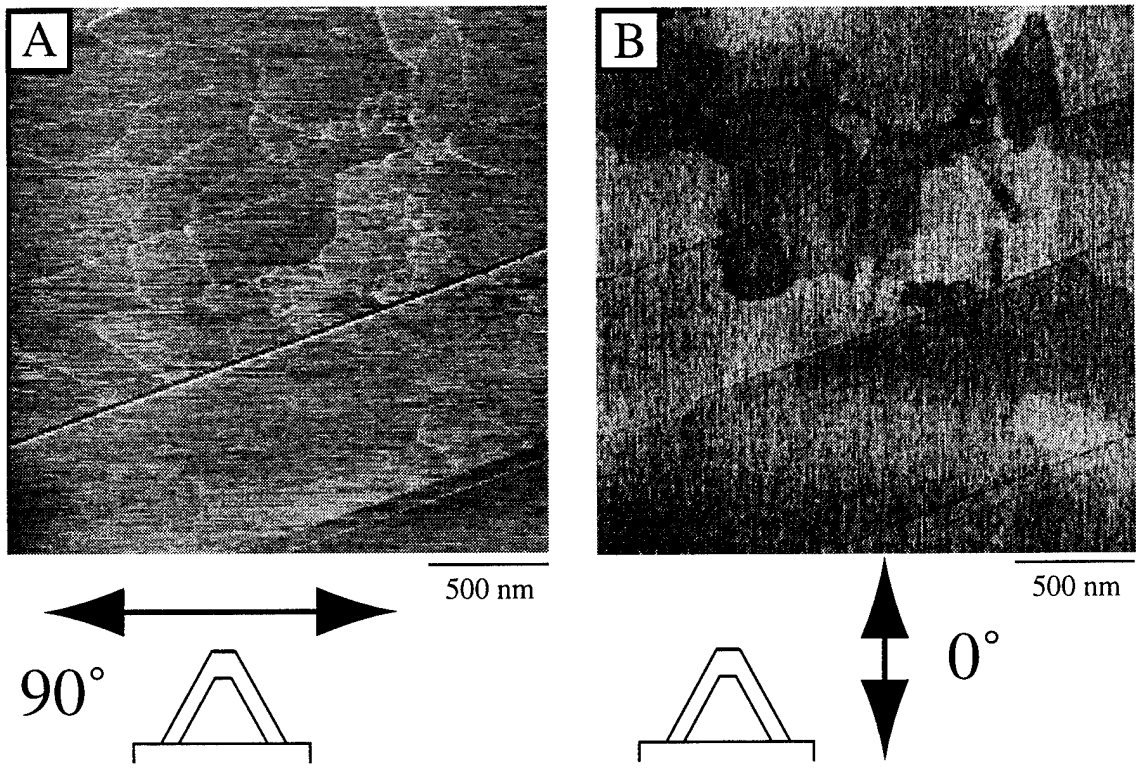
A
B
500 nm
500 nm
90°
0°

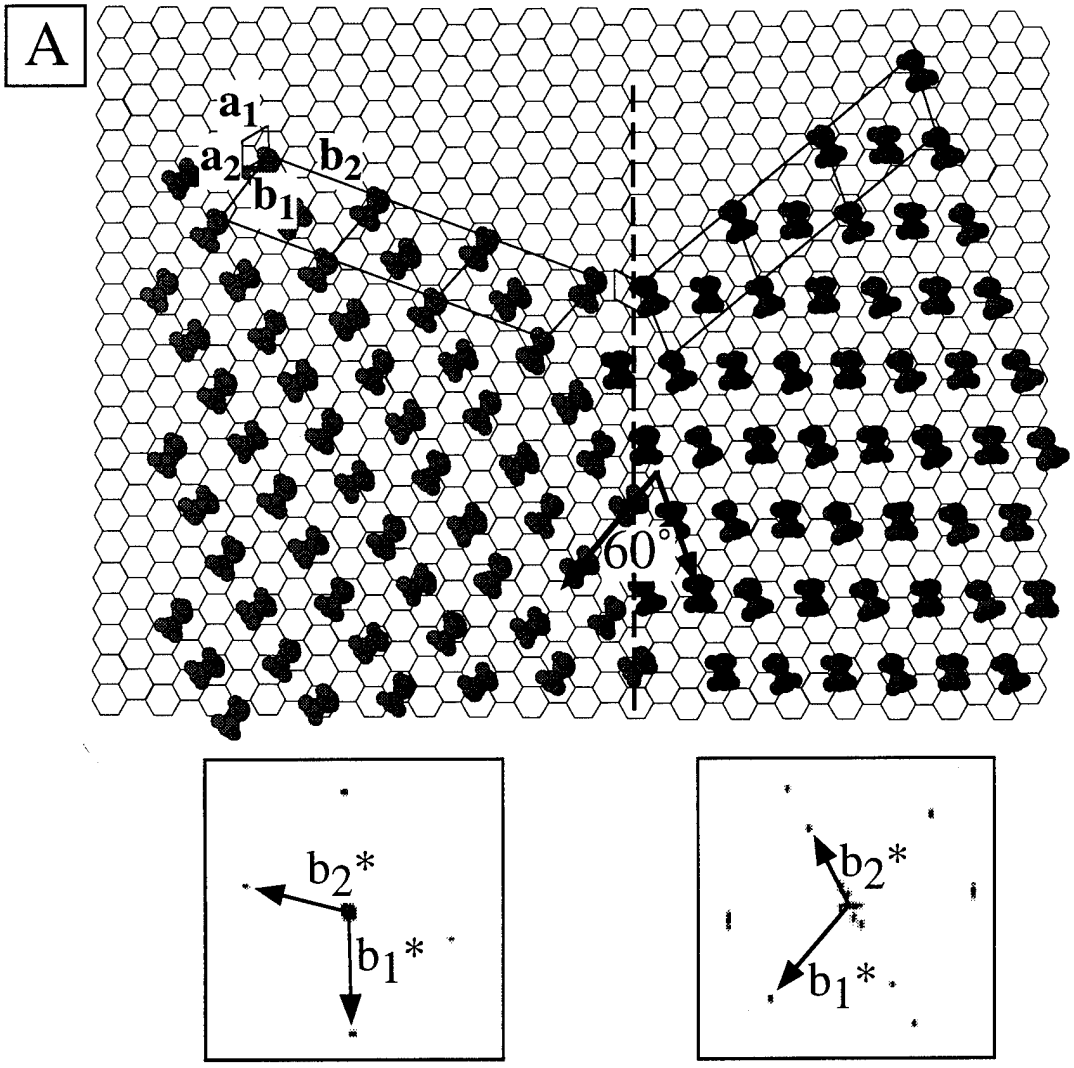
A
a1
a2
b2
b1
60°
b2*
b1*
b2*
b1*
B
0°
90°

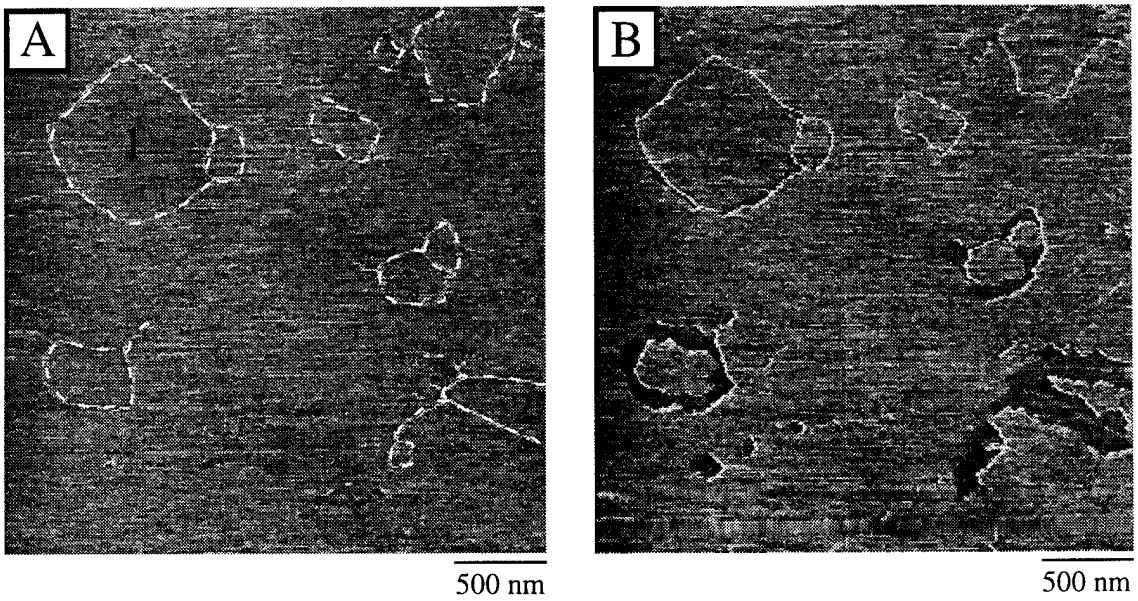
A
1
500 nm
B
500 nm

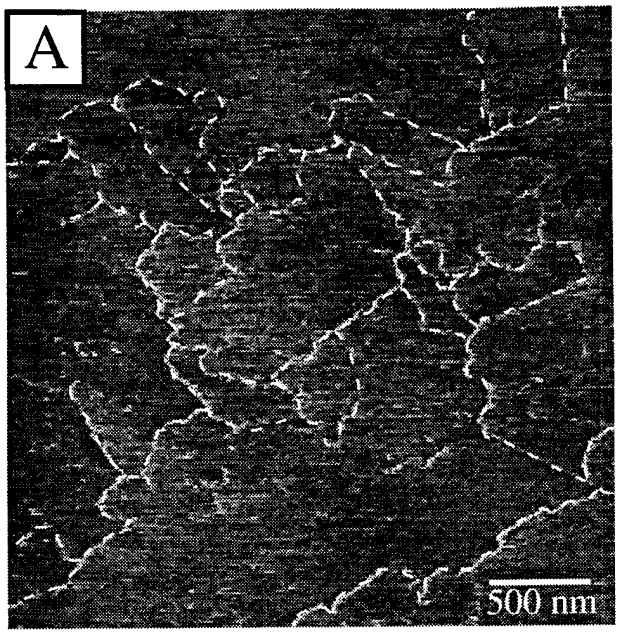
A
500 nm

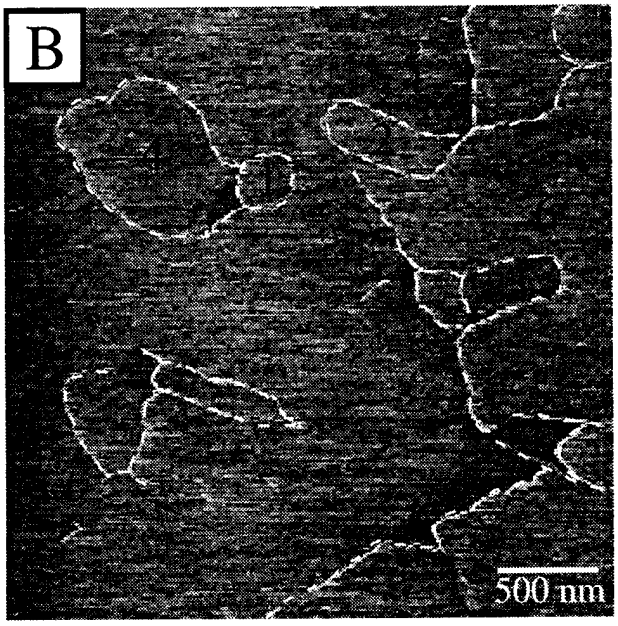
B
500 nm

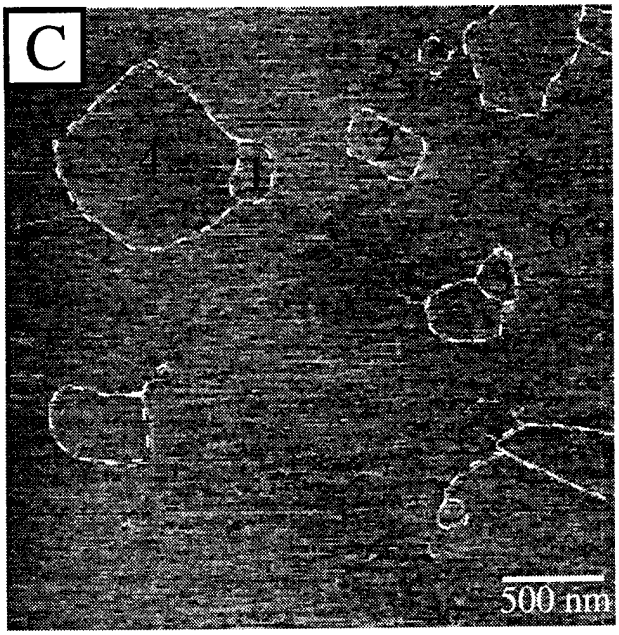
C
500 nm

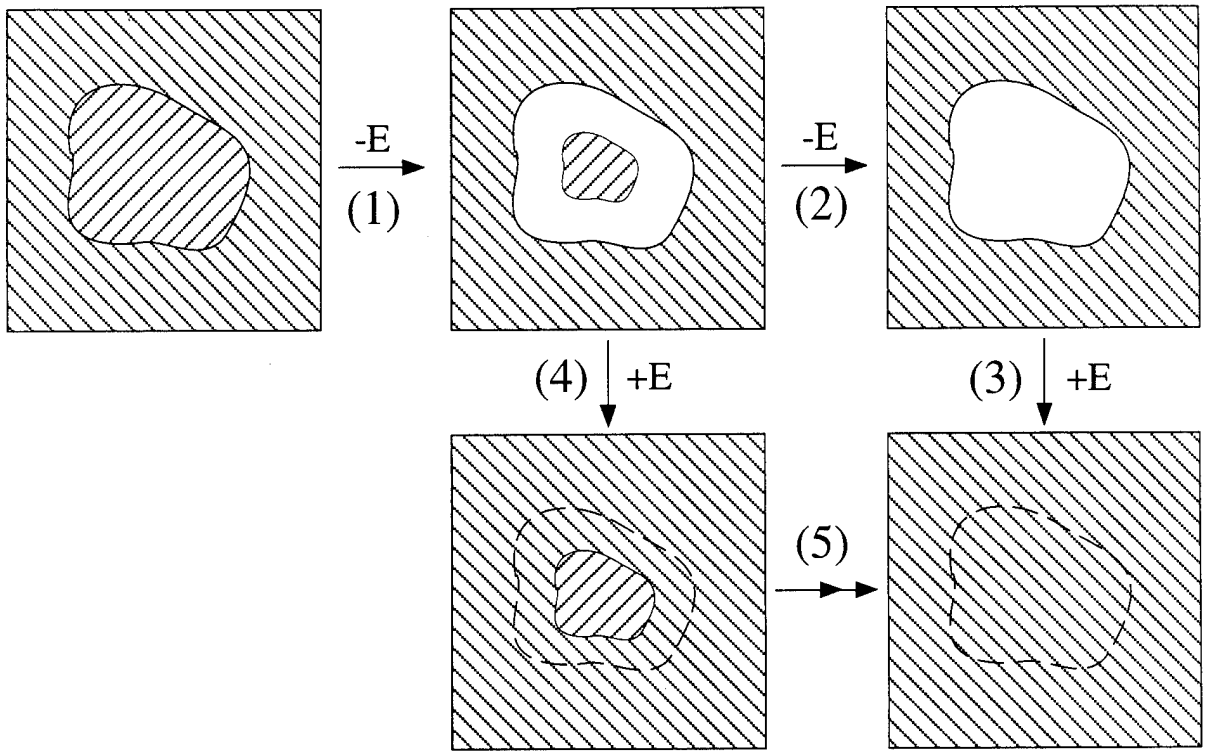
-E
(1)
-E
(2)
(4)
+E
(3)
+E
(5)